Available online at www.sciencedirect.com
SCIENCE DIRECT®
Composite Structures 69 (2005) 449–457
COMPOSITE STRUCTURES
www.elsevier.com/locate/compstruct

Static analysis of functionally graded plates using third-order shear deformation theory and a meshless method

A.J.M. Ferreira [a,*], R.C. Batra [b], C.M.C. Roque [a], L.F. Qian [c], P.A.L.S. Martins [a]

[a] Departamento de Engenharia Mecânica e Gestão Industrial, Faculdade de Engenharia da Universidade do Porto, Rua Dr. Roberto Frias, Porto 4200-465, Portugal
[b] Department of Engineering Science and Mechanics, MC 0219, Virginia Polytechnic Institute and State University, Blacksburg, VA 24061, USA
[c] Nanjing University of Science and Technology, Nanjing 210094, PR China

Available online 13 September 2004

Abstract

The collocation multiquadric radial basis functions are used to analyze static deformations of a simply supported functionally graded plate modeled by a third-order shear deformation theory. The plate material is made of two isotropic constituents with their volume fractions varying only in the thickness direction. The macroscopic response of the plate is taken to be isotropic and the effective properties of the composite are derived either by the rule of mixtures or by the Mori–Tanaka scheme. Effects of aspect ratio of the plate and the volume fractions of the constituents on the centroidal deflection are scrutinized. When Poisson's ratios of the two constituents are nearly equal, then the two homogenization techniques give results that are close to each other. However, for widely varying Poisson's ratios of the two constituents, the two homogenization schemes give quite different results. The computed results are found to agree well with the solution of the problem by an alternative meshless method.
© 2004 Elsevier Ltd. All rights reserved.

Keywords: Static analysis; Functionally graded materials; Thick plate; Meshless methods; Multiquadric radial basis functions

1. Introduction

An advantage of a plate made of a functionally graded material (FGM) over a laminated plate is that material properties vary continuously in a FGM but are discontinuous across adjoining layers in a laminated plate. It eliminates at least the delamination mode of failure. Furthermore, in an FGM, material properties can be tailored to optimize the desired characteristics, e.g., minimize the maximum deflection for a given type of loads and boundary conditions, or maximize the first frequency of free vibration of the structure. Even though material properties may vary continuously in all three directions, here we limit ourselves to analyzing static deformations of a FG plate with material properties varying only in the thickness direction.

Several investigators, e.g., see [1–4], have analyzed deformations of a FG plate either by using a plate theory or three-dimensional equations of linear elasticity for an inhomogeneous body. Exact solutions for static and dynamic deformations of a FG plate are given in [5–8]. Here we use a meshless method and a third-order shear deformation plate theory. We note that Qian et al. [9–11] used the meshless local Petrov–Galerkin method (MLPG) and either two-dimensional equations of thermoelasticity or a higher-order shear and normal deformable plate theory of Batra and Vidoli [12] to analyze static and dynamic deformations of a FG plate. The MLPG method does not need even a background mesh but requires integration over a local subdomain and the determination of basis functions by say the moving least

* Corresponding author. Tel.: +351 22 957 8713; fax: +351 22 953 7352.
E-mail address: ferreia@fe.up.pt (A.J.M. Ferreira).

0263-8223/$ - see front matter © 2004 Elsevier Ltd. All rights reserved.
doi:10.1016/j.compstruct.2004.08.003

squares method [13]. Thus, it is computationally expensive. Here we use the collocation method and the multiquadric radial basis functions which neither require a mesh nor the numerical evaluation of integrals over any subdomain. The goal here is to show that this meshless method gives results close to the analytical solution of the problem for a FG plate. No attempt has been made to review all of the literature on meshless methods, plate theories, homogenization techniques to deduce effective properties of a composite from those of its constituents, methods of manufacturing a FG plate, and papers dealing with the analysis of FG plates.

Meshless methods for finding an approximate solution of a boundary-value problem include the element-free Galerkin [14], hp-clouds [15], the reproducing kernel particle [16], the smoothed particle hydrodynamics [17], the diffuse element [18], the partition of unity finite element [19], the natural element [20], meshless Galerkin using radial basis functions [21], the meshless local Petrov–Galerkin [22], the collocation technique employing radial basis functions [23], and the modified smoothed particle hydrodynamics [24]. Of these, the last three and the smoothed particle hydrodynamics method do not require any mesh whereas others generally need a background mesh for the evaluation of integrals appearing in the weak formulation of the problem. Ferreira [25,26] has used the collocation method with the radial basis functions to analyze several plate and beam problems. The applicability of the method is extended here to analyze static deformations of a thick FG plate with a third-order shear deformation plate theory (TSDT).

The paper is organized as follows. Section 2 briefly reviews the finite point multiquadric method of solving an elliptic linear boundary-value problem. Equations for a TSDT are derived in Section 3, and two homogenization techniques for determining effective material properties of a composite are summarized in Section 4. Section 5 discusses results and Section 6 gives conclusions.

2. The finite point multiquadric method

Consider the following linear elliptic boundary-value problem defined on a smooth domain Ω:

$$\begin{aligned} Lu(\mathbf{x}) &= s(\mathbf{x}), \quad \mathbf{x} \in \Omega, \\ Bu(\mathbf{x}) &= f(\mathbf{x}), \quad \mathbf{x} \in \partial\Omega, \end{aligned} \tag{2.1}$$

where $\partial\Omega$ is the boundary of Ω, L and B are linear differential operators, and s and f are smooth functions defined on Ω and $\partial\Omega$ respectively. We select N_B points ($\mathbf{x}^{(j)}$, $j = 1, \ldots, N_B$) on $\partial\Omega$ and $(N - N_B)$ points ($\mathbf{x}^{(j)}, j = N_B + 1, N_B + 2, \ldots, N$) in the interior of Ω. Let

$$u^h(\mathbf{x}) = \sum_{j=1}^{N} a_j g(\|\mathbf{x} - \mathbf{x}^{(j)}\|, c) \tag{2.2}$$

be an approximate solution of the boundary-value problem where $a_1, a_2, \ldots, a_N$ are constants to be determined, $\|\mathbf{x} - \mathbf{x}^{(j)}\|$ is the Euclidean distance between points $\mathbf{x}$ and $\mathbf{x}^{(j)}$, c is a constant, and g is a function of $\|\mathbf{x} - \mathbf{x}^{(j)}\|$ and c. Different forms of functions g and names associated with them are

$$\begin{aligned} &\text{Multiquadrics:} \\ &g_j(\mathbf{x}) = (\|\mathbf{x} - \mathbf{x}^{(j)}\|^2 + c^2)^{1/2}, \\ &\text{Inverse Multiquadrics:} \\ &g_j(\mathbf{x}) = (\|\mathbf{x} - \mathbf{x}^{(j)}\|^2 + c^2)^{-1/2}, \\ &\text{Gaussian:} \\ &g_j(\mathbf{x}) = \mathrm{e}^{-c^2\|\mathbf{x} - \mathbf{x}^{(j)}\|^2}, \\ &\text{Thin plate splines:} \\ &g_j(\mathbf{x}) = \|\mathbf{x} - \mathbf{x}^{(j)}\|^2 \log \|\mathbf{x} - \mathbf{x}^{(j)}\|. \end{aligned} \tag{2.3}$$

Substitution from (2.2) into (2.1) and evaluating the resulting form of Eq. $(2.1)_2$ at the N_B points $\mathbf{x}^{(j)}$, $j = 1, 2, \ldots, N_B$, and of Eq. $(2.1)_1$ at $(N - N_B)$ points $\mathbf{x}^{(j)}$, $j = N_B + 1, N_B + 2, \ldots, N$ give the following N algebraic equations for the determination of $a_1, a_2, \ldots, a_N$.

$$\begin{aligned} &\sum_{j=1}^{N} a_j Lg(\|\mathbf{x} - \mathbf{x}^{(j)}\|, c)\Big|_{\mathbf{x}=\mathbf{x}^{(i)}} = s(\mathbf{x}^{(i)}), \\ &\quad i = N_B + 1, N_B + 2, \ldots, N, \\ &\sum_{j=1}^{N} a_j Bg(\|\mathbf{x} - \mathbf{x}^{(j)}\|, c)\Big|_{\mathbf{x}=\mathbf{x}^{(i)}} = f(\mathbf{x}^{(i)}), \\ &\quad i = 1, 2, \ldots, N_B. \end{aligned} \tag{2.4}$$

Depending upon the value of the parameter c and the form of function g, the set of Eqs. (2.4) that determines $a_1, a_2, \ldots, a_N$ may become ill-conditioned; e.g. see [27]. Also, the computational effort involved in solving (2.4) for $a_1, a_2, \ldots, a_N$ varies with the choice of the function g. Once Eqs. (2.4) have been solved for a's, then the approximate solution of the problem is given by (2.2).

3. Review of the third-order shear deformation plate theory

The displacement field in the TSDT is given by

$$\begin{aligned} (x, y, z) &= u_0(x, y) + z\phi_x - c_1 z^3\left(\phi_x + \frac{\partial w}{\partial x}\right), \\ v(x, y, z) &= v_0(x, y) + z\phi_y - c_1 z^3\left(\phi_y + \frac{\partial w}{\partial y}\right), \\ w(x, y, z) &= w_0(x, y), \end{aligned} \tag{3.1}$$

where $c_1 = 4/(3h^2)$, h is the plate thickness, z is the coordinate in the thickness direction, and the xy-plane of the rectangular Cartesian coordinate system is located in the midplane of the plate. Functions ϕ_x and ϕ_y describe

rotations about the x- and the y-axes of a line that is along the normal to the midsurface of the plate, u_0, v_0 and w_0 give displacements of a point on the midsurface of the plate along the x-, y- and z-axes respectively. The constant c_1 is determined by requiring that the transverse shear strain vanishes on the top and the bottom surfaces of the plate. Batra and Vidoli [12] have proposed a mixed higher-order shear and normal deformable plate theory in which natural boundary conditions prescribed on the top and the bottom surfaces of the plate are exactly satisfied.

From the strain–displacement relations appropriate for infinitesimal deformations, we obtain

$$\begin{Bmatrix} e_{xx} \\ e_{yy} \\ 2e_{xy} \\ 2e_{yz} \\ 2e_{zx} \end{Bmatrix} = \begin{Bmatrix} e_{xx}^{(0)} \\ e_{yy}^{(0)} \\ 2e_{xy}^{(0)} \\ 2e_{yz}^{(0)} \\ 2e_{zx}^{(0)} \end{Bmatrix} + z \begin{Bmatrix} e_{xx}^{(1)} \\ e_{yy}^{(1)} \\ 2e_{xy}^{(1)} \\ 2e_{yz}^{(1)} \\ 2e_{zx}^{(1)} \end{Bmatrix} + z^3 \begin{Bmatrix} e_{xx}^{(2)} \\ e_{yy}^{(2)} \\ 2e_{xy}^{(2)} \\ 2e_{yz}^{(2)} \\ 2e_{zx}^{(2)} \end{Bmatrix}, \tag{3.2}$$

where

$$\begin{Bmatrix} e_{xx}^{(0)} \\ e_{yy}^{(0)} \\ 2e_{xy}^{(0)} \\ 2e_{yz}^{(0)} \\ 2e_{zx}^{(0)} \end{Bmatrix} = \begin{Bmatrix} \frac{\partial u_0}{\partial x} \\ \frac{\partial v_0}{\partial y} \\ \frac{\partial u_0}{\partial y} + \frac{\partial v_0}{\partial x} \\ \frac{\partial w_0}{\partial y} + \phi_y \\ \frac{\partial w_0}{\partial x} + \phi_x \end{Bmatrix},$$

$$\begin{Bmatrix} e_{xx}^{(1)} \\ e_{yy}^{(1)} \\ 2e_{xy}^{(1)} \\ 2e_{yz}^{(1)} \\ 2e_{zx}^{(1)} \end{Bmatrix} = \begin{Bmatrix} \frac{\partial \phi_x}{\partial x} \\ \frac{\partial \phi_y}{\partial y} \\ \frac{\partial \phi_x}{\partial y} + \frac{\partial \phi_y}{\partial x} \\ 0 \\ 0 \end{Bmatrix},$$

$$\begin{Bmatrix} e_{xx}^{(2)} \\ e_{yy}^{(2)} \\ 2e_{xy}^{(2)} \\ 2e_{yz}^{(2)} \\ 2e_{zx}^{(2)} \end{Bmatrix} = -c_1 \begin{Bmatrix} \frac{\partial \phi_x}{\partial x} + \frac{\partial^2 w_0}{\partial x^2} \\ \frac{\partial \phi_y}{\partial y} + \frac{\partial^2 w_0}{\partial y^2} \\ \frac{\partial \phi_x}{\partial y} + \frac{\partial \phi_y}{\partial x} + 2\frac{\partial^2 w_0}{\partial x \partial y} \\ \frac{3}{z}\left(\frac{\partial w_0}{\partial y} + \phi_y\right) \\ \frac{3}{z}\left(\frac{\partial w_0}{\partial x} + \phi_x\right) \end{Bmatrix}. \tag{3.3}$$

The form (3.1) of the displacement field implies that the transverse normal strain e_{zz} vanishes identically, and $e_{yz} = 0 = e_{zx}$ at $z = \pm h/2$.

Equations for the plate theory are derived by using the principle of virtual work. That is,

$$\int_\Omega [\sigma_{xx}\delta e_{xx} + \sigma_{yy}\delta e_{yy} + 2\sigma_{xy}\delta e_{xy} + 2\sigma_{yz}\delta e_{yz} + 2\sigma_{zx}\delta e_{zx}]\,\mathrm{d}V = \int_{\partial\Omega} (f_x\delta u + f_y\delta v + f_z\delta w)\,\mathrm{d}A, \tag{3.4}$$

where σ_{xx}, σ_{yy}, σ_{xy}, σ_{yz}, σ_{zx} are components of the stress, and f_x, f_y, f_z are surface tractions acting on the bounding surfaces of the plate. Note that body forces have been neglected.

Substitution from (3.2) and (3.3) into (3.4), integration of the resulting equation with respect to z from $-h/2$ to $h/2$, and recalling that δu, δv, δw, $\delta\phi_x$ and $\delta\phi_y$ are arbitrary except at points where u, v, w, ϕ_x and ϕ_y are prescribed, we obtain the following equations for the plate theory:

$$\begin{aligned} &\frac{\partial N_{xx}}{\partial x} + \frac{\partial N_{xy}}{\partial y} = 0, \quad \frac{\partial N_{xy}}{\partial x} + \frac{\partial N_{yy}}{\partial y} = 0, \\ &\frac{\partial \overline{Q}_x}{\partial x} + \frac{\partial \overline{Q}_y}{\partial y} + f = 0, \\ &\frac{\partial \overline{M}_{xx}}{\partial x} + \frac{\partial \overline{M}_{xy}}{\partial y} - \overline{Q}_x = 0, \quad \frac{\partial \overline{M}_{xy}}{\partial x} + \frac{\partial \overline{M}_{yy}}{\partial y} - \overline{Q}_y = 0, \end{aligned} \tag{3.5}$$

where

$$\begin{aligned} &\overline{M}_{\alpha\beta} = M_{\alpha\beta} - c_1 P_{\alpha\beta}, \\ &\overline{Q}_\alpha = \widehat{Q}_\alpha - 3c_1 R_\alpha, \quad \alpha, \beta = x, y, \\ &(N_{\alpha\beta}, M_{\alpha\beta}, P_{\alpha\beta}) = \int_{-h/2}^{h/2} (1, z, z^3)\sigma_{\alpha\beta}\,\mathrm{d}z, \\ &(\widehat{Q}_\alpha, R_\alpha) = \int_{-h/2}^{h/2} (1, z^2)\sigma_{\alpha z}\,\mathrm{d}z, \\ &f = f_z^+ + f_z^-, \end{aligned} \tag{3.6}$$

f_z^+ and f_z^- equal normal surface tractions acting on the top and the bottom surfaces of the plate. In this plate theory, $f_x^\pm$ and $f_y^\pm$ must identically vanish on the top and the bottom surfaces of the plate.

Expressions for $M_{\alpha\beta}$, $N_{\alpha\beta}$, $P_{\alpha\beta}$, Q_α and R_α in terms of strains can be derived by substituting into (3.6) from the following stress–strain relation for an isotropic material:

$$\begin{Bmatrix} \sigma_{xx} \\ \sigma_{yy} \\ \sigma_{xy} \\ \sigma_{yz} \\ \sigma_{zx} \end{Bmatrix} = \begin{bmatrix} Q_{11} & Q_{12} & 0 & 0 & 0 \\ Q_{12} & Q_{11} & 0 & 0 & 0 \\ 0 & 0 & Q_{33} & 0 & 0 \\ 0 & 0 & 0 & Q_{33} & 0 \\ 0 & 0 & 0 & 0 & Q_{33} \end{bmatrix} \begin{Bmatrix} e_{xx} \\ e_{yy} \\ 2e_{xy} \\ 2e_{yz} \\ 2e_{zx} \end{Bmatrix}, \tag{3.7}$$

where

$$Q_{11} = E/(1-\nu^2), \quad Q_{12} = \nu E/(1-\nu^2), \quad Q_{33} = E/2(1+\nu), \tag{3.8}$$

E is the effective Young's modulus and ν the effective Poisson's ratio at a point in a FG plate.

Substitution for strains in terms of displacements from (3.3) into (3.7), for stresses from (3.7) into (3.6),

for $M_{\alpha\beta}$, $N_{\alpha\beta}$ etc. from (3.6) into (3.5) yield equilibrium equations in terms of the generalized displacements u_0, v_0, w_0, ϕ_x and ϕ_y; these equations are summarized in Appendix A. An approximate solution of these equations and the pertinent boundary conditions is found by using the meshless method described in Section 2. That is, we assume that

$$\begin{aligned} u_0^h(\mathbf{x}) &= \sum_{j=1}^{N} a_j^u g(\|\mathbf{x}-\mathbf{x}^{(j)}\|, c), \\ v_0^h(\mathbf{x}) &= \sum_{j=1}^{N} a_j^v g(\|\mathbf{x}-\mathbf{x}^{(j)}\|, c), \text{etc.} \end{aligned} \tag{3.9}$$

These expressions are substituted in equilibrium equations listed in Appendix A, and also in relevant boundary conditions.

Boundary conditions at a simply supported edge, $x = a$, are

$$\begin{aligned} &w_0(a,y) = 0, \quad v_0(a,y) = 0, \quad \phi_y(a,y) = 0, \\ &N_{xx}(a,y) = 0, \quad \overline{M}_{xx}(a,y) = 0. \end{aligned} \tag{3.10}$$

Boundary conditions imposed at a rigidly clamped edge, $y = b$, are

$$\begin{aligned} &u_0(x,b) = 0, \quad v_0(x,b) = 0, \quad w_0(x,b) = 0, \\ &\phi_x(x,b) = 0, \quad \phi_y(x,b) = 0. \end{aligned} \tag{3.11}$$

4. Homogenization of material properties

We assume that the plate is made of two randomly distributed isotropic constituents, the macroscopic response of the composite is isotropic, and the composition of the composite varies only in the z-direction. Qian and Batra [28] have studied free vibrations of a FG plate with material properties varying smoothly in two directions. The volume fraction of constituent 1 is given by

$$V_1 = \left(\frac{1}{2} + \frac{z}{h}\right)^p. \tag{4.1}$$

Thus $V_1 = 0$ at the bottom surface $z = -h/2$ and $V_1 = 1$ at the top surface $z = h/2$ of the plate. Fig. 1 depicts the through-the-thickness distribution of the volume fraction of phase 1 for different values of p.

Two homogenization techniques are used to find the effective properties at a point. According to the rule of mixtures, the effective property P, at a point is given by

$$P = P_1 V_1 + P_2 V_2, \tag{4.2}$$

where V_1 and $V_2 = 1 - V_1$ are the volume fractions of constituents 1 and 2 respectively, and P_1 and P_2 are values of P for the two constituents.

According to the Mori–Tanaka [29] homogenization method the effective bulk modulus, K, and the effective shear modulus, G, of the composite are given by

$$\begin{aligned} \frac{K-K_1}{K_2-K_1} &= \frac{V_2}{1+(1-V_2)\frac{K_2-K_1}{K_1+\frac{4}{3}G_1}}, \\ \frac{G-G_1}{G_2-G_1} &= \frac{V_2}{1+(1-V_2)\frac{G_2-G_1}{G_1+f_1}}, \end{aligned} \tag{4.3}$$

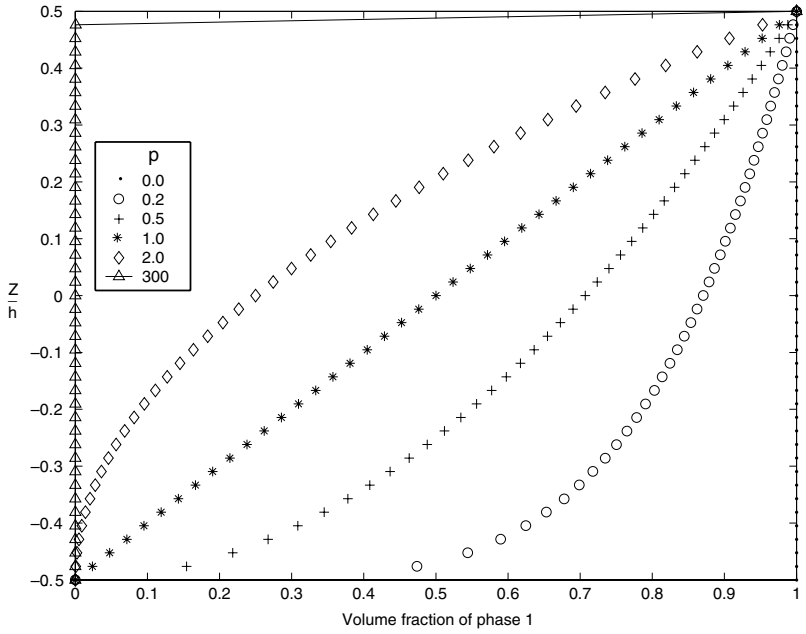

Fig. 1. Through-the-thickness distribution of the volume fraction of phase 1 for different values of the exponent p in Eq. (4.1).

where $f_1 = \frac{G_1(9K_1+8G_1)}{6(K_1+2G_1)}$. The effective values of Young's modulus, E, and Poisson's ratio, ν, are found from

$$E = \frac{9KG}{3K+G}, \quad \nu = \frac{3K-2G}{2(3K+G)}. \tag{4.4}$$

5. Computation and discussion of results

The results for a simply-supported FG plate comprised of aluminum ($E_1 = 70\,\text{GPa}$, $\nu_1 = 0.3$) and a ceramic ($E_2 = 151\,\text{GPa}$, $\nu_2 = 0.3$) are firstly compared and then for an aluminum/silicon carbide plate; for SiC, $E = 427\,\text{GPa}$, $\nu = 0.17$. The first composite material is referred to as FGM1 and the second as FGM2. Computed results for the FGM2 plate are compared with the solution of Qian et al. [9]. In the Tables and Figures to follow, the vertical or transverse displacement w, the axial stress σ_{xx}, the thickness coordinate z, and the pressure q applied on the top surface of the plate have been non-dimensionalized as follows:

$$\bar{w} = w/h, \quad \bar{\sigma}_{xx} = \sigma_{xx}/q, \quad \bar{q} = q/E_1 h^4, \quad \bar{z} = z/h.$$

Henceforth the superimposed bar has been dropped. Results are presented for a square plate and equal number of collocation points uniformly spaced in the x- and the y-directions are used. We employ multiquadrics radial basis functions defined by Eq. (2.3) $_1$ with c equal to either $1/\sqrt{N_a}$ or $2/\sqrt{N_a}$ where N_a is the number of collocation points in either x- or y-direction.

Fig. 2a and b depicts, for $p = 0$, 1, 2 and 6 in Eq. (4.1), the through-the-thickness variations of the effective Young's modulus, and the effective Poisson's ratio as computed by the rule of mixtures and the Mori–Tanaka scheme for the FGM2 plates. For both FGM1 and FGM2 plates, and with $p = 2$, values of the effective moduli obtained from the rule of mixture differ noticeably from those derived from the Mori–Tanaka scheme; the difference between the two sets of moduli for other values of p are less evident.

For $N_a = 11$ and 19, we have compared in Table 1 the centroidal deflections of a simply supported square FGM1 plate. For $p = 0$, 0.5, 1.0, 2.0 and ∞, the centroidal deflection computed with $N_a = 11$ differs from that computed with $N_a = 19$ by less than 1.5%. Furthermore, these deflections differ from those computed by the MLPG code of Qian, Batra and Chen [9] by less than 3%; the difference being smaller for $N_a = 19$. Results presented below have been computed with $N_a = 15$.

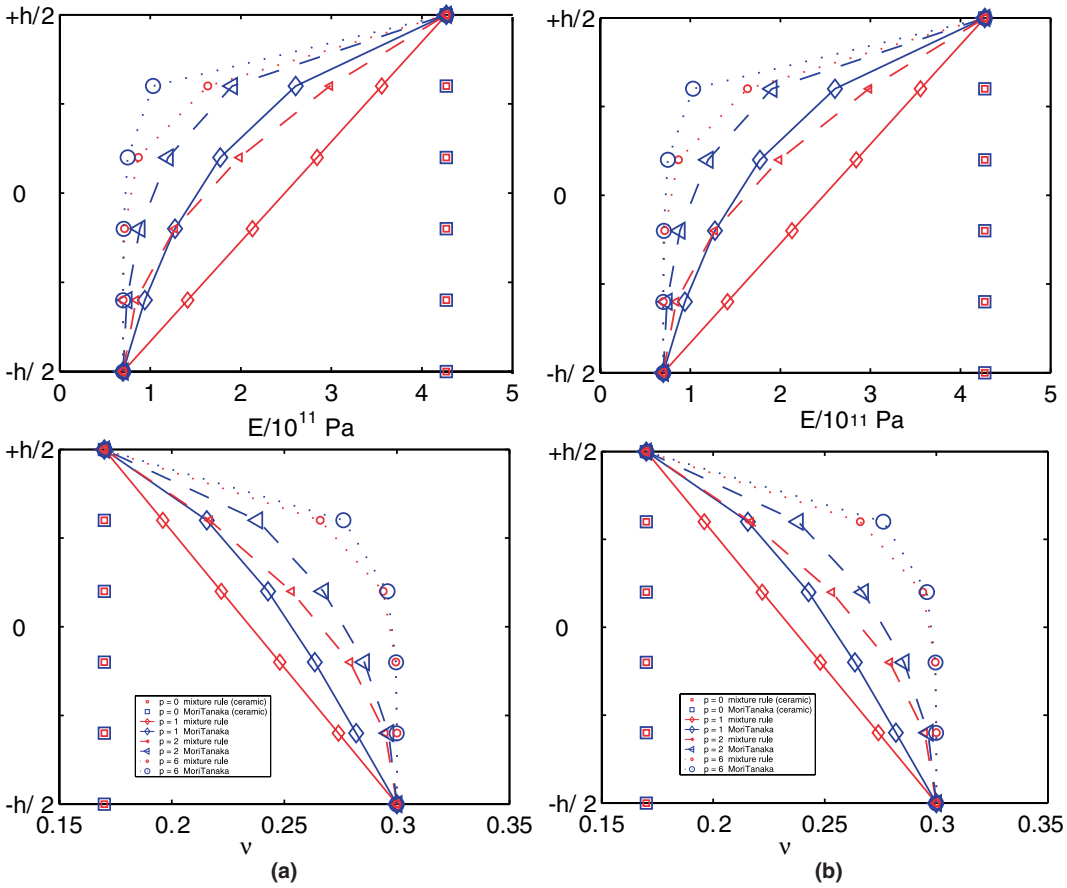

Fig. 2. Through-the-thickness variations of the effective Young's modulus, and Poisson's ratio computed by the rule of mixtures and the Mori–Tanaka scheme for (a) FGM1 and (b) FGM2 plates with $p = 0$, 1, 2 and 6 in Eq. (4.1).

Table 1
For $N_a = 11$ and 19, comparison of the centroidal deflection of a simply supported square FGM1 plate with effective elastic moduli computed by the rule of mixtures and the Mori–Tanaka scheme

Exponent, p in Eq. (4.1)	Non-dimensional centroidal deflection		
	Effective properties by rule of mixtures	Effective properties by Mori–Tanaka scheme	MLPG code of Qian, Batra and Chen
0	0.02050 (0.02080)	0.02050 (0.02080)	0.02118
0.5	0.02620 (0.02650)	0.02760 (0.02790)	–
1.0	0.02940 (0.02970)	0.03050 (0.03090)	0.03150
2.0	0.03230 (0.03240)	0.03300 (0.03330)	0.03395
Metal	0.04430 (0.0448)	0.04430 (0.04480)	0.04580

Load parameter = 1, aspect ratio a/h of plate = 20, $c = \frac{2}{\sqrt{(N_a)}}$. Results for $N_a = 19$ are in parentheses.

Table 2
For $a/h = 5$, $N_a = 15$, and load parameter = 1, comparison of the centroidal deflection of a simply supported square FGM1 and FGM2 plates with effective elastic moduli computed by the rule of mixtures and the Mori–Tanaka scheme

Exponent, p in Eq. (4.1)	Non-dimensional centroidal deflection		
	Effective properties by rule of mixtures	Effective properties by Mori–Tanaka scheme	MLPG code of Qian, Batra and Chen
(a) FGM1			
0.0	0.02477	0.02477	0.02436
0.5	0.03135	0.03293	–
1.0	0.03515	0.03666	0.03634
2.0	0.03883	0.04009	0.03976
Metal	0.05343	0.05343	0.05253
(b) FGM2			
0.0	−0.007676	−0.00909	−0.00902
0.5	−0.011973	−0.01871	–
1.0	−0.015967	−0.02381	−0.02391
2.0	−0.021603	−0.02903	−0.02918
Metal	−0.053426	−0.05343	−0.05253

For thick ($a/h = 5$) FGM1 and FGM2 simply supported square plates, Table 2 compares the centroidal deflections with effective moduli derived by the two homogenization schemes. It is transparent that the two homogenization schemes give results that are close to each other for the FGM1 plate but are quite different for the FGM2 plate. Note that Poisson's ratios of the two constituents of the FGM1 plate are nearly equal but are quite different for the FGM2 plate. Note that for each plate, the presently computed centroidal deflection compares very well with that obtained by the MLPG code of Qian, Batra and Chen [9] that uses the Mori–Tanaka homogenization scheme. Results computed with the MLPG method agreed very well with the analytical solution of Vel and Batra [5,6].

In order to delineate the effect of the parameter c in Eq. $(2.3)_1$, we have compared in Table 3 centroidal deflections of the square FGM1 plate for $c = 1/\sqrt{15}$ and $c = 2/\sqrt{15}$ with those computed from the MLPG code of Qian, Batra and Chen [9]. These results evince

Table 3
For $c = 1/\sqrt{15}$ and $2/\sqrt{15}$, comparison of the centroidal deflection of a simply supported square FGM1 plate with effective elastic moduli computed by the Mori–Tanaka scheme

a/h	MLPG, 8×8 grid				Present formulation; $c = \frac{1}{\sqrt{(N_a)}}$				$c = 2/\sqrt{N_a}$			
	$p = 0$	$p = 1.0$	$p = 2.0$	Metal	$p = 0$	$p = 1.0$	$p = 2.0$	Metal	$p = 0$	$p = 1.0$	$p = 2.0$	Metal
5	0.02436	0.03634	0.03976	0.05252	0.02475	0.03663	0.04000	0.05339	0.02476	0.03666	0.04009	0.05342
15	0.02115	0.03152	0.03401	0.04583	0.02170	0.03222	0.03470	0.04681	0.02090	0.03103	0.03354	0.04510
25	0.02123	0.03158	0.03404	0.04569	0.02277	0.03385	0.03630	0.04911	0.02062	0.03061	0.03305	0.04448
45	0.02158	0.03203	0.03456	0.04655	0.02679	0.03990	0.04237	0.05779	0.02057	0.03054	0.03295	0.04437
75	0.02190	0.03252	0.03501	0.04728	0.03677	0.05495	0.05721	0.07932	0.02062	0.03061	0.03302	0.04448
125	0.02225	0.03304	0.03562	0.04802	0.09117	0.13876	0.13020	0.19668	0.02069	0.03072	0.03314	0.04464

Load factor = −1.

Table 4
Comparison of the stress σ_{xx} at the centroids of the top and the bottom surfaces of a simply supported square FGM1 plate with effective elastic moduli computed by the Mori–Tanaka scheme from the present formulation and the MLPG code of Qian, Batra and Chen [9]

Index p or aspect ratio a/h	MLPG, 8×8 grid		Present formulation	
	$\sigma_{xx}(-h/2)$	$\sigma_{xx}(h/2)$	$\sigma_{xx}(-h/2)$	$\sigma_{xx}(h/2)$
$p = 0$ (ceramic)	0.29175	−0.29200	0.28650	−0.28650
$p = 1$	0.22617	−0.37875	0.17815	−0.38428
$p = 2$	0.24497	−0.40650	0.21278	−0.45899
$p = \infty$ (metal)	0.29175	−0.29200	0.28650	−0.28650
$a/h = 5$	0.22540	−0.38812	0.20232	−0.43643
$a/h = 10$	0.22420	−0.37760	0.19812	−0.42737
$a/h = 15$	0.22502	−0.37742	0.19738	−0.42577
$a/h = 20$	0.22617	−0.37875	0.19719	−0.42537
$a/h = 200$	0.02331	−0.38980	0.19841	−0.42800

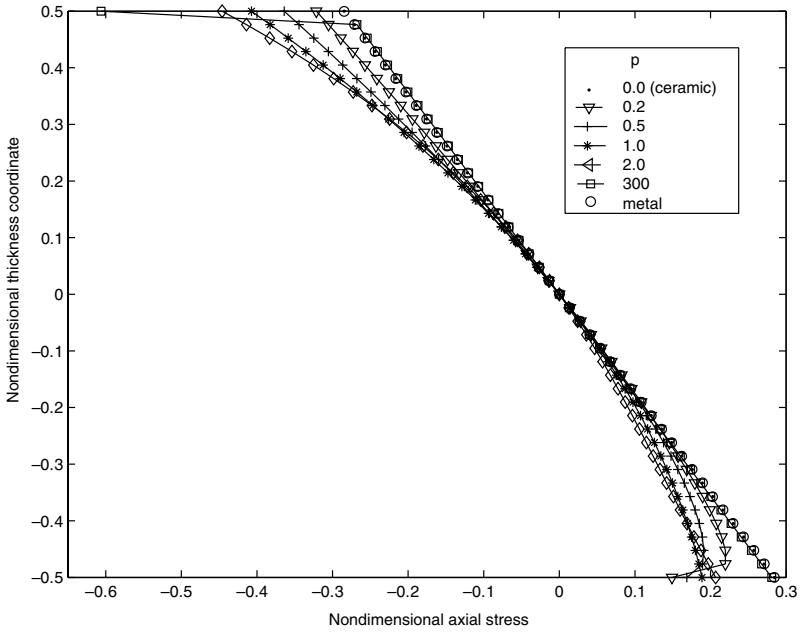

Fig. 3. Through-the-thickness variation of the axial stress, σ_{xx}, in a simply supported FGM1 plate for different values of the exponent p in Eq. (4.1).

that $c = 2/\sqrt{15}$ should be used for thin plates. For plates with $a/h \leqslant 15$, $c = 1/\sqrt{15}$ gives good results and the accuracy of the computed centroidal deflection deteriorates with an increase in the aspect ratio. We note that Fasshauer's [23] suggestion of using $c = 2/\sqrt{N_a}$ is supported by our numerical experiments.

For different values of the index p in Eq. (4.1) and the aspect ratio a/h, Table 4 compares the axial stress, σ_{xx}, at centroids of the top and the bottom surfaces of the simply supported square FGM1 plate. The stress computed from the present formulation compares well with that obtained from the MLPG code of Qian, Batra and Chen [9].

Fig. 3 exhibits through-the-thickness variation of the non-dimensional axial stress σ_{xx}. Except for very large or very small values of p, the axial stress varies smoothly through the plate thickness. For $p = 0.2$, there is a sharp gradient in σ_{xx} near the bottom surface of the plate, and for $p = 300$ there is a steep gradient in σ_{xx} near the top surface. This is caused by the sharp variation in the material properties near the top and the bottom surfaces of the plate for $p = 0.2$ and 300.

6. Conclusions

The meshless collocation method, the multiquadric radial basis functions and a third-order shear deformation theory have been used to analyze static deformations of functionally graded square plates of different aspect ratios. Two homogenization techniques, namely, the rule of mixture and the Mori–Tanaka scheme, have been used to find effective moduli of the composite. Computed results are found to agree well with those

obtained from the meshless local Petrov–Galerkin (MLPG) code of Qian, Batra and Chen. Both the collocation and the MLPG methods result in asymmetric "stiffness" matrices. The CPU time required to solve the problem with the collocation method is considerably less than that needed for the MLPG code mainly because no numerical integration is needed in the collocation scheme.

For widely varying Poisson's ratios of the two constituents of the FG plate, the two homogenization techniques give quite different results. Our numerical experiments suggest that the parameter c in the expression for the multiquadratic radial basis functions should equal $2/\sqrt{N_a}$ where N_a equals the number of collocation points in the x- or the y-direction.

Appendix A

Equations for the determination of the generalized displacements u_0, v_0, w_0, ϕ_x and ϕ_y of a TSDT are listed below.

$$\begin{aligned}
&A_{11}\frac{\partial^2 u_o}{\partial x^2}+A_{12}\frac{\partial^2 v_o}{\partial y\partial x}+B_{11}\frac{\partial^2 \phi_x}{\partial x^2}+B_{12}\frac{\partial^2 \phi_y}{\partial y\partial x}\\
&-\frac{4}{3h^2}E_{11}\left(\frac{\partial^2 \phi_x}{\partial x^2}+\frac{\partial^3 w_o}{\partial x^3}\right)-\frac{4}{3h^2}E_{12}\left(\frac{\partial^2 \phi_y}{\partial y\partial x}+\frac{\partial^3 w_o}{\partial y^2\partial x}\right)\\
&+A_{33}\left(\frac{\partial^2 u_o}{\partial y^2}+\frac{\partial^2 v_o}{\partial y\partial x}\right)+B_{33}\left(\frac{\partial^2 \phi_x}{\partial y^2}+\frac{\partial^2 \phi_y}{\partial y\partial x}\right)\\
&-\frac{4}{3h^2}E_{33}\left(\frac{\partial^2 \phi_x}{\partial y^2}+\frac{\partial^2 \phi_y}{\partial y\partial x}+2\frac{\partial^3 w_o}{\partial y^2\partial x}\right)=0, \qquad (A.1)
\end{aligned}$$

$$\begin{aligned}
&A_{33}\left(\frac{\partial^2 u_o}{\partial y\partial x}+\frac{\partial^2 v_o}{\partial x^2}\right)+B_{33}\left(\frac{\partial^2 \phi_x}{\partial y\partial x}+\frac{\partial^2 \phi_y}{\partial x^2}\right)\\
&-\frac{4}{3h^2}E_{33}\left(\frac{\partial^2 \phi_x}{\partial y\partial x}+\frac{\partial^2 \phi_y}{\partial x^2}+2\frac{\partial^3 w_o}{\partial y\partial x^2}\right)+A_{12}\frac{\partial^2 u_o}{\partial y\partial x}\\
&+A_{22}\frac{\partial^2 v_o}{\partial y^2}+B_{12}\frac{\partial^2 \phi_x}{\partial y\partial x}+B_{22}\frac{\partial^2 \phi_y}{\partial y^2}\\
&-\frac{4}{3h^2}E_{12}\left(\frac{\partial^2 \phi_x}{\partial y\partial x}+\frac{\partial^3 w_o}{\partial y\partial x^2}\right)\\
&-\frac{4}{3h^2}E_{22}\left(\frac{\partial^2 \phi_y}{\partial y^2}+\frac{\partial^3 w_o}{\partial y^3}\right)=0, \qquad (A.2)
\end{aligned}$$

$$\begin{aligned}
&A_{55}\left(\frac{\partial \phi_x}{\partial x}+\frac{\partial^2 w_o}{\partial x^2}\right)-\frac{8}{h^2}D_{55}\left(\frac{\partial \phi_x}{\partial x}+\frac{\partial^2 w_o}{\partial x^2}\right)\\
&+\frac{16}{h^4}F_{55}\left(\frac{\partial \phi_x}{\partial x}+\frac{\partial^2 w_o}{\partial x^2}\right)+A_{44}\left(\frac{\partial \phi_y}{\partial y}+\frac{\partial^2 w_o}{\partial y^2}\right)\\
&-\frac{8}{h^2}D_{44}\left(\frac{\partial \phi_y}{\partial y}+\frac{\partial^2 w_o}{\partial y^2}\right)+\frac{16}{h^4}F_{44}\left(\frac{\partial \phi_y}{\partial y}+\frac{\partial^2 w_o}{\partial y^2}\right)\\
&+\frac{4}{3}\left[E_{11}\frac{\partial^3 u_o}{\partial x^3}+E_{12}\frac{\partial^3 v_o}{\partial y\partial x^2}+F_{11}\frac{\partial^3 \phi_x}{\partial x^3}+F_{12}\frac{\partial^3 \phi_y}{\partial y\partial x^2}\right.\\
&-\frac{4}{3h^2}H_{11}\left(\frac{\partial^3 \phi_x}{\partial x^3}+\frac{\partial^4 w_o}{\partial x^4}\right)-\frac{4}{3h^2}H_{12}\left(\frac{\partial^3 \phi_y}{\partial y\partial x^2}+\frac{\partial^4 w_o}{\partial y^2\partial x^2}\right)\\
&+2E_{33}\left(\frac{\partial^3 u_o}{\partial y^2\partial x}+\frac{\partial^3 v_o}{\partial y\partial x^2}\right)+2F_{33}\left(\frac{\partial^3 \phi_x}{\partial y^2\partial x}+\frac{\partial^3 \phi_y}{\partial y\partial x^2}\right)\\
&-\frac{8}{3h^2}H_{33}\left(\frac{\partial^3 \phi_x}{\partial y^2\partial x}+\frac{\partial^3 \phi_y}{\partial y\partial x^2}+2\frac{\partial^4 w_o}{\partial y^2\partial x^2}\right)+E_{12}\frac{\partial^3 u_o}{\partial y^2\partial x}\\
&+E_{22}\frac{\partial^3 v_o}{\partial y^3}+F_{12}\frac{\partial^3 \phi_x}{\partial y^2\partial x}+F_{22}\frac{\partial^3 \phi_y}{\partial y^3}-\frac{4}{3h^2}H_{12}\\
&\left.\times\left(\frac{\partial^3 \phi_x}{\partial y^2\partial x}+\frac{\partial^4 w_o}{\partial y^2\partial x^2}\right)-\frac{4}{3h^2}H_{22}\left(\frac{\partial^3 \phi_y}{\partial y^3}+\frac{\partial^4 w_o}{\partial y^4}\right)\right]\frac{1}{h^2}\\
&=-q_0, \qquad (A.3)
\end{aligned}$$

$$\begin{aligned}
&-A_{55}\left(\phi_x+\frac{\partial w_o}{\partial x}\right)+\frac{8}{h^2}D_{55}\left(\phi_x+\frac{\partial w_o}{\partial x}\right)\\
&-\frac{16}{h^4}F_{55}\left(\phi_x+\frac{\partial w_o}{\partial x}\right)+B_{11}\frac{\partial^2 u_o}{\partial x^2}+B_{12}\frac{\partial^2 v_o}{\partial y\partial x}+D_{11}\frac{\partial^2 \phi_x}{\partial x^2}\\
&+D_{12}\frac{\partial^2 \phi_y}{\partial y\partial x}-\frac{4}{3h^2}F_{11}\left(\frac{\partial^2 \phi_x}{\partial x^2}+\frac{\partial^3 w_o}{\partial x^3}\right)\\
&-\frac{4}{3h^2}F_{12}\left(\frac{\partial^2 \phi_y}{\partial y\partial x}+\frac{\partial^3 w_o}{\partial y^2\partial x}\right)-\frac{4}{3}\left[E_{11}\frac{\partial^2 u_o}{\partial x^2}+E_{12}\frac{\partial^2 v_o}{\partial y\partial x}\right.\\
&+F_{11}\frac{\partial^2 \phi_x}{\partial x^2}+F_{12}\frac{\partial^2 \phi_y}{\partial y\partial x}-\frac{4}{3h^2}H_{11}\left(\frac{\partial^2 \phi_x}{\partial x^2}+\frac{\partial^3 w_o}{\partial x^3}\right)\\
&\left.-\frac{4}{3h^2}H_{12}\left(\frac{\partial^2 \phi_y}{\partial y\partial x}+\frac{\partial^3 w_o}{\partial y^2\partial x}\right)\right]\frac{1}{h^2}+B_{33}\left(\frac{\partial^2 u_o}{\partial y^2}+\frac{\partial^2 v_o}{\partial y\partial x}\right)\\
&+D_{33}\left(\frac{\partial^2 \phi_x}{\partial y^2}+\frac{\partial^2 \phi_y}{\partial y\partial x}\right)-\frac{4}{3h^2}F_{33}\\
&\times\left(\frac{\partial^2 \phi_x}{\partial y^2}+\frac{\partial^2 \phi_y}{\partial y\partial x}+2\frac{\partial^3 w_o}{\partial y^2\partial x}\right)-\frac{4}{3}\left[B_{33}\left(\frac{\partial^2 u_o}{\partial y^2}+\frac{\partial v_o}{\partial y\partial x}\right)\right.\\
&+F_{33}\left(\frac{\partial^2 \phi_x}{\partial y^2}+\frac{\partial^2 \phi_y}{\partial y\partial x}\right)-\frac{4}{3h^2}H_{33}\left(\frac{\partial^2 \phi_x}{\partial y^2}+\frac{\partial^2 \phi_y}{\partial y\partial x}\right.\\
&\left.\left.+2\frac{\partial^3 w_o}{\partial y^2\partial x}\right)\right]\frac{1}{h^2}=0, \qquad (A.4)
\end{aligned}$$

$$\begin{aligned}
&-A_{44}\left(\phi_y+\frac{\partial w_o}{\partial y}\right)+\frac{8}{h^2}D_{44}\left(\phi_y+\frac{\partial w_o}{\partial y}\right)\\
&-\frac{16}{h^4}F_{44}\left(\phi_y+\frac{\partial w_o}{\partial y}\right)+B_{12}\frac{\partial^2 u_o}{\partial y\partial x}+B_{22}\frac{\partial^2 v_o}{\partial y^2}+D_{12}\frac{\partial^2 \phi_x}{\partial y\partial x}\\
&+D_{22}\frac{\partial^2 \phi_y}{\partial y^2}-\frac{4}{3h^2}F_{12}\left(\frac{\partial^2 \phi_x}{\partial y\partial x}+\frac{\partial^3 w_o}{\partial y\partial x^2}\right)
\end{aligned}$$

$$-\frac{4}{3h^2}F_{22}\left(\frac{\partial^2\phi_y}{\partial y^2}+\frac{\partial^3 w_o}{\partial y^3}\right)-\frac{4}{3}\left[E_{12}\frac{\partial^2 u_o}{\partial y\partial x}+E_{22}\frac{\partial^2 v_o}{\partial y^2}+F_{12}\frac{\partial^2\phi_x}{\partial y\partial x}+F_{22}\frac{\partial^2\phi_y}{\partial y^2}-\frac{4}{3h^2}H_{12}\left(\frac{\partial^2\phi_x}{\partial y\partial x}+\frac{\partial^3 w_o}{\partial y\partial x^2}\right)-\frac{4}{3h^2}H_{22}\left(\frac{\partial^2\phi_y}{\partial y^2}+\frac{\partial^3 w_o}{\partial y^3}\right)\right]\frac{1}{h^2}+B_{33}\left(\frac{\partial^2 u_o}{\partial y\partial x}+\frac{\partial^2 v_o}{\partial x^2}\right)+D_{33}\left(\frac{\partial^2\phi_x}{\partial y\partial x}+\frac{\partial^2\phi_y}{\partial x^2}\right)-\frac{4}{3h^2}F_{33}\left(\frac{\partial^2\phi_x}{\partial y\partial x}+\frac{\partial^2\phi_y}{\partial x^2}+2\frac{\partial^3 w_o}{\partial y\partial x^2}\right)-\frac{4}{3}\left[E_{33}\left(\frac{\partial^2 u_o}{\partial y\partial x}+\frac{\partial^2 v_o}{\partial x^2}\right)+F_{33}\left(\frac{\partial^2\phi_x}{\partial y\partial x}+\frac{\partial^2\phi_y}{\partial x^2}\right)-\frac{4}{3h^2}H_{33}\left(\frac{\partial^2\phi_x}{\partial y\partial x}+\frac{\partial^2\phi_y}{\partial x^2}+2\frac{\partial^3 w_o}{\partial y\partial x^2}\right)\right]\frac{1}{h^2}=0, \tag{A.5}$$

where

$$(A_{ij},B_{ij},D_{ij},E_{ij},F_{ij},H_{ij})=\int_{-\frac{h}{2}}^{+\frac{h}{2}}\left((P_t-P_b)\left(\frac{z}{h}+\frac{1}{2}\right)^p(1,z,z^2,z^3,z^4,z^6)+Q_b(1,z,z^2,z^3,z^4,z^6)\right)\mathrm{d}z. \tag{A.6}$$

References

[1] Reddy JN. Analysis of functionally graded plates. Int J Numer Methods Eng 2000;47:663–84.

[2] Cheng ZQ, Batra RC. Deflection relationships between the homogeneous Kirchhoff plate theory and different functionally graded plate theories. Arch Mech 2000;52:143–58.

[3] Tarn JQ, Wang YM. Asymptotic thermoelastic analysis of anisotropic inhomogeneous and laminated plates. J Thermal Stresses 1995;18:35–58.

[4] Cheng ZQ, Batra RC. Three-dimensional thermoelastic deformations of a functionally graded elliptic plate. Composites B 2000; 31:97–106.

[5] Vel SS, Batra RC. Exact thermoelasticity solution for cylindrical bending deformations of functionally graded plates. In: Proceedings of the IUTAM Symposium on Dynamics of Advanced Materials and Smart Structures, Yonezawa, Japan, May 20–24, 2003.

[6] Vel SS, Batra RC. Exact solution for thermoelastic deformations of functionally graded thick rectangular plates. AIAA J 2002;40: 1421–33.

[7] Vel SS, Batra RC. Three-dimensional exact solution for the vibration of functionally graded rectangular plates. J Sound Vibration 2004;272(3–5):703–30.

[8] Vel SS, Mewer R, Batra RC. Analytical solution for the cylindrical bending vibration of piezoelectric composite plates. Int J Solids Struct 2004;41:1625–43.

[9] Qian LF, Batra RC, Chen LM. Static and dynamic deformations of thick functionally graded elastic plate by using higher-order shear and normal deformable plate theory and meshless local Petrov–Galerkin method. Composites Part B Engineering 2004;35(6–8):685–97.

[10] Qian LF, Batra RC, Chen LM. Analysis of cylindrical bending thermoelastic deformations of functionally graded plates by a meshless local Petrov–Galerkin method. Comput Mech 2004; 33(4):263–73.

[11] Qian LF, Batra RC. Transient thermoelastic deformations of a thick functionally graded plate. J Thermal Stresses 2004;27(8): 705–40.

[12] Batra RC, Vidoli S. Higher order piezoelectric plate theory derived from a three-dimensional variational principle. AIAA J 2002;40(1):91–104.

[13] Lancaster P, Salkauskas K. Surfaces generated by moving least squares methods. Math Comput 1981;37:141–58.

[14] Belytschko T, Lu YY, Gu L. Element-free Galerkin methods. Int J Numer Methods Eng 1994;37:229–56.

[15] Duarte CA, Oden JT. H–p clouds—an *hp* meshless method. Numer Methods Partial Differential Equations 1996:1–34.

[16] Liu WK, Jun S, Zhang Y. Reproducing kernel particle method. Int J Numer Methods Eng 1995;20:1081–106.

[17] Lucy LB. A numerical approach to the testing of the fission hypothesis. Astronom J 1977;82(12):1013–24.

[18] Nayroles B, Touzot G, Villon P. Generalizing the finite element method: diffuse approximation and diffuse elements. Comput Mech 1992;10:307–18.

[19] Melenk JM, Babuska I. The partition of unity finite element method: basic theory and applications. Comput Methods Appl Mech Eng 1996;139:289–314.

[20] Sukumar N, Moran B, Belytschko T. The natural element method in solid mechanics. Int J Numer Methods Eng 1998;43:839–87.

[21] Wendland H. Piecewise polynomial positive, definite and compactly supported radial basis functions of minimal degree. Adv Comput Methods 1995;4:389–96.

[22] Atluri SN, Zhu T. A new Meshless Local Petrov–Galerkin (MLPG) approach in computational mechanics. Comput Mech 1998;22(2):117–27.

[23] Fasshauer GE. Solving partial differential equations by collocation with radial basis functions. In: Proceedings of the 3rd International Conference on Curves and Surfaces, Surface Fitting and Multiresolution Methods, vol. 2, 1997, p. 131–8.

[24] Zhang GM, Batra RC. Modified smoothed particle hydrodynamics method and its application to transient problems. Comput Mech 2004;34(2):137–46.

[25] Ferreira AJM. A formulation of the multiquadric radial basis function method for the analysis of laminated composite plates. Compos Struct 2003;59:385–92.

[26] Ferreira AJM. Thick composite beam analysis using a global meshless approximation based on radial basis function. Mech Adv Mater Struct 2003;10(4):395–401.

[27] Liu GR. Meshfree methods, moving beyond the finite element method. CRC Press; 2002.

[28] Qian LF, Batra RC. Design of bidirectional functionally graded plate for optimal natural frequencies. J Sound Vib, in press.

[29] Mori T, Tanaka K. Average stress in matrix and average elastic energy of materials with misfitting inclusions. Acta Metall 1973; 21:571–4.